ornl

NUREG/CR-4039
ORNL/TM-9440

OAK RIDGE
NATIONAL
LABORATORY

MARTIN MARIETTA

Gamma-Ray Characterization of the Two-Year Irradiation Experiment Performed at the Poolside Facility

R. E. Maerker

Prepared for the
U.S. Nuclear Regulatory Commission
Office of Nuclear Regulatory Research
Under Interagency Agreement DOE 40-551-75

OPERATED BY
MARTIN MARIETTA ENERGY SYSTEMS, INC.
FOR THE UNITED STATES
DEPARTMENT OF ENERGY

NOTICE

Availability of Reference Materials Cited in NRC Publications

Most documents cited in NRC publications will be available from one of the following sources:

1. The NRC Public Document Room, 1717 H Street, N.W., Washington, DC 20555
2. The NRC/GPO Sales Program, U.S. Nuclear Regulatory Commission, Washington, DC 20555
3. The National Technical Information Service, Springfield, VA 22161

Although the listing that follows represents the majority of documents cited in NRC publications, it is not intended to be exhaustive.

Referenced documents available for inspection and copying for a fee from the NRC Public Document Room include NRC correspondence and internal NRC memoranda; NRC Office of Inspection and Enforcement bulletins, circulars, information notices, inspection and investigation notices; Licensee Event Reports; vendor reports and correspondence; Commission papers; and applicant and licensee documents and correspondence.

The following documents in the NUREG series are available for purchase from the NRC/GPO Sales Program: formal NRC staff and contractor reports, NRC-sponsored conference proceedings, and NRC booklets and brochures. Also available are Regulatory Guides, NRC regulations in the *Code of Federal Regulations*, and *Nuclear Regulatory Commission Issuances*.

Documents available from the National Technical Information Service include NUREG series reports and technical reports prepared by other federal agencies and reports prepared by the Atomic Energy Commission, forerunner agency to the Nuclear Regulatory Commission.

Documents available from public and special technical libraries include all open literature items, such as books, journal and periodical articles, and transactions. *Federal Register* notices, federal and state legislation, and congressional reports can usually be obtained from these libraries.

Documents such as theses, dissertations, foreign reports and translations, and non-NRC conference proceedings are available for purchase from the organization sponsoring the publication cited.

Single copies of NRC draft reports are available free, to the extent of supply, upon written request to the Division of Technical Information and Document Control, U.S. Nuclear Regulatory Commission, Washington, DC 20555.

Copies of industry codes and standards used in a substantive manner in the NRC regulatory process are maintained at the NRC Library, 7920 Norfolk Avenue, Bethesda, Maryland, and are available there for reference use by the public. Codes and standards are usually copyrighted and may be purchased from the originating organization or, if they are American National Standards, from the American National Standards Institute, 1430 Broadway, New York, NY 10018.

NUREG/CR-4039
ORNL/TM-9440
Distribution Category R5

Engineering Physics and Mathematics Division

GAMMA-RAY CHARACTERIZATION OF THE TWO-YEAR IRRADIATION EXPERIMENT PERFORMED AT THE POOLSIDE FACILITY

R. E. Maerker

NRC Monitor: C. Z. Serpan
Nuclear Regulatory Commission
Washington, DC 20555

Project Manager: F. B. K. Kam
Oak Ridge National Laboratory

Principal Investigator: R. E. Maerker
Oak Ridge National Laboratory

Document Issued: January 1985

This Work Performed for
Nuclear Regulatory Commission
Under
DOE Interagency Agreement 40-551-75
NRC Fin No. B0415

Prepared by the
Oak Ridge National Laboratory
Oak Ridge, Tennessee 37831
operated by
Martin Marietta Energy Systems, Inc.
for the
U.S. DEPARTMENT OF ENERGY
under Contract No. DE-AC05-840R21400

TABLE OF CONTENTS

LIST OF FIGURES

LIST OF TABLES

LIST OF TABLES (cont'd)

ABSTRACT

Average gamma-ray group fluence rates are calculated for each of the three exposures in the two-year metallurgical blind test experiment at the ORR-Poolside Facility in Oak Ridge, thus completing the characterization of the radiation field for this experiment, which is intended to serve as an international metallurgical benchmark. Heating rates in the steel derived from these calculations varied from about 0.23 watts/gram in the simulated surveillance capsule to 1.4 milliwatts/gram at the three-quarters depth location in the simulated pressure vessel capsule, with secondaries arising from non-fission reactions in the core and ex-core steel contributing between seventy-seven and ninety-three percent of the total. Contributions from photofission to fission foil activities are estimated to be less than five percent of those previously calculated arising from neutron-induced fission.

EXECUTIVE SUMMARY

Average gamma-ray group fluence rates are presented for each of three exposures (two surveillance capsules and a pressure vessel capsule) and five locations (center of the surveillance capsule and near surface, one-quarter, half- and three-quarter depths into the pressure vessel capsule) in the two-year metallurgical blind test experiment performed at the ORR-Poolside Facility in Oak Ridge. This experiment is intended to serve as an international metallurgical benchmark, and the present analysis completes the description of the radiation field - the gamma-ray characterization presented in this report serving as a complement to the neutron characterization presented in an earlier one.

In contrast to the neutron analysis, however, the gamma-ray fluence rates were calculated for only one fission source distribution in the core (i.e., that previously calculated for the scoping startup experiment) and then scaled to the blind test exposures on the basis of factors inferred from the earlier neutron analysis.

The group fluence rates were decomposed into three components - those due to prompt fission gamma rays in the core, those from fission-product decay gamma rays (also in the core), and those arising from neutron interactions other than fission throughout both the core and the aluminum, steel, and water configuration beyond the core.

The effects of the finite core height on the fluence rates throughout the configuration were obtained from a combination of various one- and two-dimensional discrete ordinate calculations in a fluence-rate synthesis procedure previously adopted for neutrons. These effects were found to approach reduction factors of two for the non-fission component at the three-quarter depth location. Somewhat smaller effects were calculated for the two fission gamma-ray components.

Heating rates in the steel indicate a range of values lying between about 0.23 watts/gram in the surveillance capsule to 1.4 milliwatts/gram at the three-quarter depth inside the pressure vessel capsule. The most significant contributor to the heating rates is the component arising as secondaries from neutron interactions other than fission - most probably thermal-neutron capture in the capsules - which account for between seventy-seven and ninety-three percent of the total deposited energy.

Reaction rates due to photofission contributions in the fission foils at the various locations throughout the configuration were also estimated and compared with the previously calculated neutron-induced reaction rates and found to be non-negligible only for the case of ^{238}U at the near-surface location in the pressure vessel capsule, where it amounted to a little less than five percent.

GAMMA-RAY CHARACTERIZATION OF THE TWO-YEAR IRRADIATION EXPERIMENT PERFORMED AT THE POOLSIDE-FACILITY

INTRODUCTION

The two-year metallurgical "blind test" irradiations performed at the Poolside Facility (PSF) in Oak Ridge during the period May 1980 - June 1982 have been previously characterized as to the neutron field (1). A similar characterization for gamma rays is also desirable, since photofission contributions to fission foil activities and heating rates arising from gamma-ray energy deposition in the metallurgical samples are of interest as well. Although the samples were maintained at a near-constant temperature by means of specially designed temperature controls, the heating calculations are important to the estimating of the amount of coolant that must be made available in any future constant temperature exposures.

Because of the nature of the two-year exposures - they arose from using 52 cycles of the Oak Ridge Research Reactor (ORR) that produced variable fluence rate levels - a procedure for the calculation of the gamma-rays similar to the one previously adopted for the calculation of the neutrons was dismissed as being too expensive. It was decided that a calculation of the startup experiment (a single cycle scoping replica of the blind test experiment) would go a long way toward estimating the gamma-ray fields in the blind test exposures. Further, the results of the previous neutron calculations showed that the relative neutron spectra were independent of fuel cycle, and it can be argued that the relative gamma spectra should also be independent of fuel cycle since they arise from the same fission distributions that give rise to the neutrons. Thus gamma-ray fluxes for the blind test exposures can be estimated by scaling the fluxes calculated in the startup experiment using factors derived from the earlier neutron analysis.

There are two possible objections to scaling the gamma-ray levels in the startup and blind test exposures with the same factors that can be derived from the neutron analysis. The first objection is that carbon steel specimens in the blind test capsules replaced the stainless steel used throughout the startup configurations. This significant change in the two geometries, along with the less significant substitution of water for air in the "void box" backing the simulated pressure vessel in the blind test, can affect the source of secondary gamma-rays arising from neutron interactions in the steel. This objection can be removed by performing the startup calculations with the blind test materials in place of their startup counterparts. (It will subsequently be shown that this substitution has very little effect on the neutron transport through the simulated pressure vessel.) The second objection is that the gamma rays arising from fission-product decay in the reactor possibly produce different relative flux levels (and spectra) with fuel cycle than the neutrons or other gamma rays do because of the different time histories of the fissions that have occurred in the various fuel elements comprising the core. This objection can be dispensed with at once for two reasons - the magnitude of the decay gamma rays decreases rapidly with increasing time after fission, and the contribution of even the

"short-term" (<9 days after fission) component which dominates this particular source is virtually negligible compared with those from other gamma-ray sources, as will be shown later on.

The rationale for the particular method adopted for these calculations having now been presented, details of the calculations will appear in the following sections.

Cross Sections Used

The basic cross section library used for these calculations is SAILOR (2), which is a coupled 47 neutron - 20 gamma-ray group library devised by SAI, ORNL and EPRI for use in light water reactors. The version of SAILOR adopted for the present study contains revised thermal cross sections calculated by M. L. Williams, then of ORNL. These better thermal values differed by ~5% or less from the original SAILOR values, but were based on collapsing from a one-dimensional calculation involving many thermal groups with upscattering. The library contains neither beryllium nor cadmium, so that the reflector and control rod regions of the ORR core could not be accurately described in the transport calculation. However, the fission source distribution in the core was based on the same diffusion theory calculation employing VENTURE (3) that was used in the previous neutron field characterization of the startup experiment (1). The neglect of the cadmium entirely and the replacement of the missing beryllium cross sections with those of water of density 1.5 g/cm^3 (approximately matching the total cross sections of beryllium in the MeV range) should introduce only a small uncertainty into the calculation of all ex-core fluxes except those in the immediate vicinity of the beryllium blocks (see Figs. 1 and 2). A quantitative measure of the perturbations introduced by these approximations along with the substitution of carbon steel for stainless steel (see Introduction) appears in Table 1, where dosimeter responses obtained with the SAILOR library and materials are compared with those obtained with the ELXSIR library and materials used in the earlier neutron characterization startup analysis (1). It can be concluded that the two neutron calculations agree to within about 5%, the discrepancy being due not only to material substitutions but also to differences in the libraries of materials common to both sets.

The gamma-ray production cross sections for ^{235}U in the SAILOR library contain the prompt component from fission. This is a complication if one wishes to separate the contributions to the ex-core gamma-ray fluxes into their prompt and non-fission-related components.‡ (Fission

‡The attempt to separate out these two components by running two transport calculations, one including and the other not including the uranium cross sections, would yield invalid conclusions because the thermal flux would not be the same in the two cases and as a consequence the in-core capture gamma rays in the aluminum and water would be different - being suppressed when the uranium was present at the expense of the uranium fission and capture gamma rays.

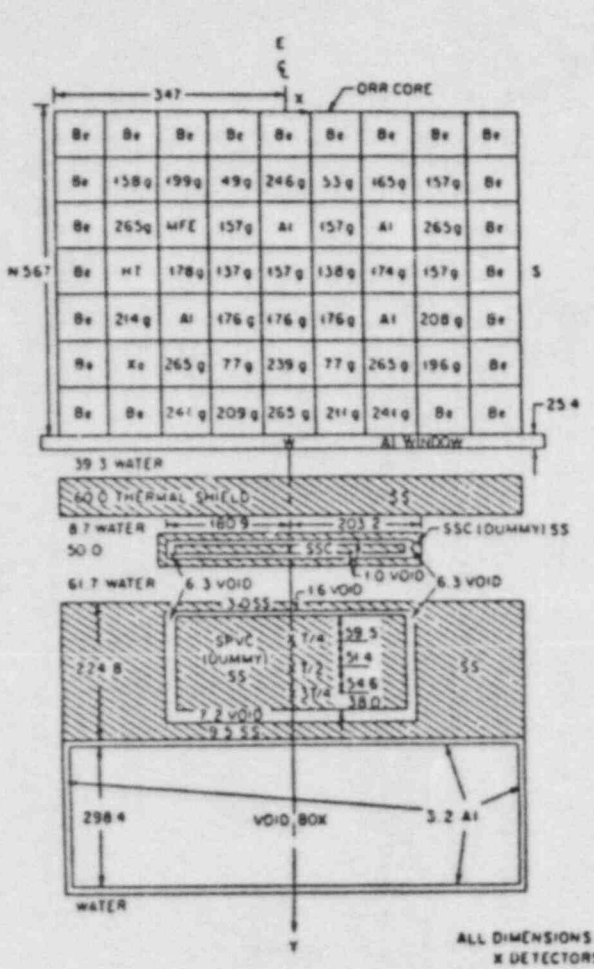

Fig. 1. Horizontal (XY) Cut at Location of Maximum Axial Flux of ORR-PSF Startup Experiment.

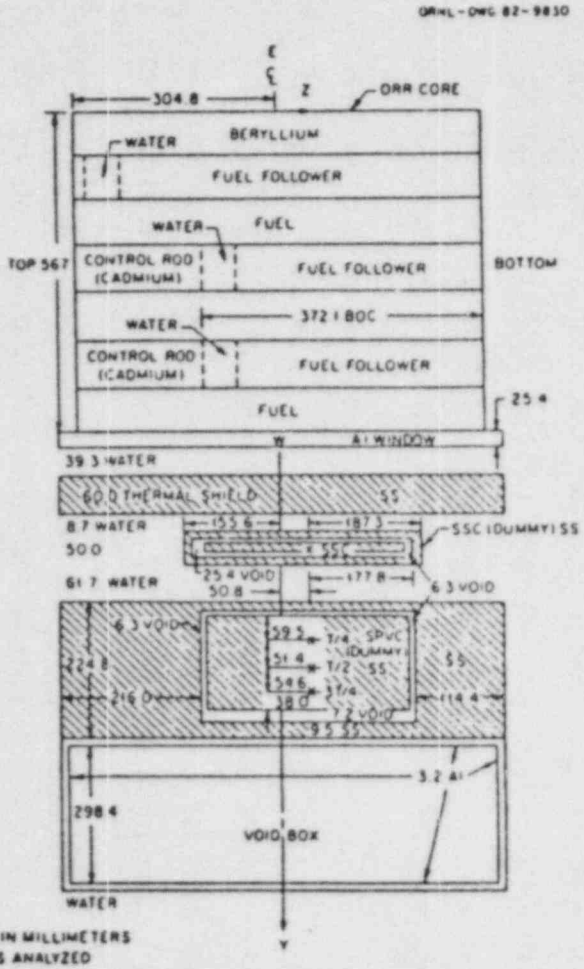

Fig. 2. Vertical (YZ) Cut at Location of Radial Centerline of ORR-PSF Startup Experiment.

Table 1. Gross Neutron Response Comparisons Between Startup Calculations Using SAILOR (S) and ELXSIR (E) Libraries*

	$[R_{XY}]_S$	$[R_{XY}]_E$	S/E	$[R_{YZ}]_S$	$[R_{YZ}]_E$	S/E	$[R_Y]_S$	$[R_Y]_E$	S/E
				$^{63}Cu(n,\alpha)$					
SSC ℄	2.52(-13)†	2.52(-13)	1.00	2.37(-13)	2.32(-13)	1.02	5.26(-12)	5.12(-12)	1.03
OT	2.60(-14)	2.60(-14)	1.00	2.48(-14)	2.43(-14)	1.02	5.90(-13)	5.75(-13)	1.03
T/4 ℄	2.51(-14)	2.53(-14)	0.99	9.14(-15)	9.01(-15)	1.01	2.27(-13)	2.23(-13)	1.02
T/2	9.46(-15)	9.57(-15)	0.99	9.14(-15)	9.01(-15)	1.01	2.27(-13)	2.23(-13)	1.02
3T/4	3.[illegible](-15)	3.40(-15)	0.99	3.27(-15)	3.23(-15)	1.01	8.26(-14)	8.12(-14)	1.02
				$^{54}Fe(n,p)$					
SSC	3.80(-11)	3.87(-11)	0.98	3.50(-11)	3.49(-11)	1.00	7.59(-10)	7.51(-10)	1.01
OT	3.14(-12)	3.19(-12)	0.98	2.96(-12)	2.94(-12)	1.01	6.85(-11)	6.75(-11)	1.02
T/4 ℄	3.10(-12)	3.15(-12)	0.98	2.95(-12)	2.92(-12)	1.01	6.98(-11)	6.86(-11)	1.02
T/2	1.15(-12)	1.16(-12)	0.99	1.10(-12)	1.09(-12)	1.01	2.66(-11)	2.60(-11)	1.02
3T/4	3.97(-13)	3.98(-13)	1.00	3.84(-13)	3.76(-13)	1.02	9.43(-12)	9.16(-12)	1.03
				$^{237}Np(n,f)$					
SSC	1.54(-9)	1.64(-9)	0.94	1.40(-9)	1.48(-9)	0.95	3.08(-8)	3.14(-8)	0.98
OT	9.20(-11)	9.69(-11)	0.95	8.59(-11)	8.77(-11)	0.98	2.02(-9)	2.04(-9)	0.99
T/4 ℄	1.64(-10)	1.75(-10)	0.94	1.52(-10)	1.60(-10)	0.95	3.83(-9)	3.90(-9)	0.98
T/2	9.24(-11)	9.87(-11)	0.94	8.84(-11)	9.12(-11)	0.97	2.28(-9)	2.33(-9)	0.98
3T/4	4.73(-11)	4.98(-11)	0.95	4.52(-11)	4.64(-11)	0.97	1.22(-9)	1.24(-9)	0.98

*All entries are integrated over the detector volumes and the full core.
†Read 2.52×10^{-13} reactions per second per nucleus x cm^3, etc.

product gamma rays can be handled separately.) The complication arises because the ex-core gamma-ray sources are calculated from the slowing down of the source input to the transport code (i.e., from a VENTURE diffusion theory calculated fission distribution), whereas the in-core thermal-capture gamma-rays and those from prompt fission are determined from thermal-neutron fluxes and a fission distribution calculated by the transport code in the slowing down from the VENTURE distribution. The slowing down and original fission distributions are not expected to be identical because the transport calculation uses only two thermal groups, whereas the diffusion theory calculation uses several additional thermal groups with upscattering included. Furthermore, the uranium must be modeled as a material in the transport calculation if the prompt component is to be included. Thus, to separate out the prompt gamma-ray contributions from the remainder, one must first be assured that the transport calculated slowing down fission distribution starting from the VENTURE distribution is reasonably close to the original VENTURE distribution. If it is, then the prompt gamma-ray contribution obtained by using the original VENTURE distribution in a gamma-only transport calculation with a supplied prompt gamma-ray spectrum can be subtracted from the results of the coupled calculation using the VENTURE neutron source alone to yield the non-fission-related component.

Since the assumption that the prompt gamma-ray component obtained in the coupled calculation is reasonably close to that obtained in the gamma-only calculation rests on an adequate comparison of the VENTURE and transport calculated, i.e., DOT(4), neutron source density distributions, Table 2 is presented which shows the two spatial distributions in the outermost (i.e., "A") row of the ORR core loading used in cycle 151A for the startup experiment (see Figs. 1 and 2).

In Table 2, the element numbers A3-A7 are superimposed on the table entries to orient the reader, with Y interval = 24 corresponding to the outside and Y = 22 the inside of the fuel element. X interval = 9 corresponds to the right most edge of the first row fuel in Fig. 1, etc., when viewed reading the figure title. A comparison of the entries shows a maximum discrepancy in element A5, which is a fresh fuel region. Overall, the average of the three outer interval ratios, V/D, is 0.84, which is considered adequate agreement in view of the fact that the non-fission-related gamma rays dominate the coupled calculation.

One more caveat regarding the cross sections in the coupled calculation must be mentioned. The standard procedure for obtaining a three-dimensional flux from one- and two-dimensional transport calculations involves integrating the VENTURE source over the third dimension (in the case of the one-dimensional calculation over the second and third dimensions). The prompt gamma rays in the coupled calculation arise from neutron interaction with the fuel, which to be consistent should be represented by cross sections integrated over the same dimensions. Doing this, however, would result in fuel cross-sections that are unrealistically large and attenuating. Since the neutrons are attenuated by only an average fuel concentration, not an integral concentration, the easiest

Table 2. Comparison of XY Neutron Source Densities Integrated Over Z Calculated by VENTURE(V) and Recalculated by DOT(D), in Units of 10^{15} neutrons/cm^2/sec

Yint	Xint	9	10	11	12	13	14	15	16	17	18	19	20
24	V	1.32	1.23	1.25	1.14	1.15	1.17	1.17	1.14	1.13	1.33	1.28	1.26
	D	1.46	1.22	1.32	1.25	1.28	1.32	1.38	1.41	1.45	1.92	1.96	1.83
23	V	1.41	1.29	1.30	1.19	1.20	1.23	1.22	1.19	1.17	1.35	1.30	1.29
	D	1.69	1.14	1.27	1.20	1.25	1.27	1.34	1.39	1.44	1.92	1.97	1.83
22	V	1.54	1.43	1.44	1.33	1.35	1.39	1.39	1.34	1.31	1.52	1.46	1.44
	D	1.92	1.50	1.65	1.56	1.61	1.66	1.69	1.68	1.68	2.09	2.04	1.98

Yint	Xint	21	22	23	24	25	26	27	28	29
24	V	1.02	1.02	1.02	0.97	0.93	0.91	0.98	0.92	0.97
	D	1.34	1.29	1.24	1.15	1.08	1.05	1.08	0.94	1.06
23	V	1.05	1.05	1.06	1.01	0.95	0.93	0.99	0.94	1.05
	D	1.33	1.27	1.19	1.07	1.02	0.97	1.00	0.86	1.16
22	V	1.17	1.18	1.19	1.13	1.07	1.04	1.09	1.04	1.19
	D	1.54	1.52	1.49	1.39	1.31	1.25	1.27	1.13	1.48

way to ensure consistency between the prompt source and non-fission-related source without distorting the transport is to use VENTURE sources averaged over the third dimensions in conjunction with uranium cross sections based on concentrations also averaged over the third dimensions. The flux synthesis procedure then involves the following combination:

$$\phi_g(x,y,z) = \phi_g(x,y)\phi_g(y,z)/\phi_g(y) \quad , \tag{1}$$

where the fluxes on the right hand side of Eq. (1) are solutions using as sources

$$S(x,y) = \int_0^{60.96} S(x,y,z)dz \; / \; 60.96 \quad , \tag{2}$$

$$S(y,z) = \int_0^{53.34} S(x,y,z)dx \; / \; 53.34 \quad , \tag{3}$$

and

$$S(y) = \int_0^{53.34} dx \int_0^{60.96} S(x,y,z)dz \; / \; (60.96)(53.34) \quad , \tag{4}$$

respectively, where the height of the active ORR core is 60.96 cm and the width 53.34 cm.

The average uranium concentration in each fuel element was obtained from estimating the middle-of-cycle mass distributions of fuel present in the loading of cycle 151A. Averages for each row for the YZ calculations, for each element for the XY calculations, and for each depth for the Y calculations were computed and the corresponding macroscopic cross sections obtained.

Iron Heating Response

Gamma-ray energy absorption response cross sections in iron were taken to be the Kerma factors for iron that are part of the BUGLE-80 library (5), whose gamma-ray group structure is identical to the one used in SAILOR. These cross sections treat bremsstrahlung and fluorescence radiation as absorption, allowing only Compton scattered and annihilation radiation to escape. This is consistent with the transport cross section treatment in which transfer matrices via these latter two processes are explicitly retained. The values in Ref. (5) are given in units of MeV barns/atom, which must be multiplied by

$$10^{-24}\text{cm}^2/\text{barn} \times 1.602 \times 10^{-6}\text{ergs/MeV} \times \frac{0.6023\times10^{24}}{55.85}\ \text{atoms/g iron} = 1.728\times10^{-8}$$

to convert to units of cm^2 ergs/g iron.

Table 3 presents these cross sections in three different units. The last column is expressed in units of cm^2/g iron, which can be derived from the original units of MeV barns/atom by multiplying by

$$10^{-24} cm^2/barn \times \frac{1}{\bar{E}} MeV^{-1} \times \frac{0.6023 \times 10^{24}}{55.85} atoms/g\ iron = \frac{.01078}{\bar{E}(MeV)} .$$

The total gamma-ray energy absorbed is obtained most conveniently from the folding of H_g in units of cm^2 ergs/gram with ϕ_g in units of photons/cm^2/sec to yield the heating rate in units of ergs/gram/sec, or if divided by 10^7, in units of watts/gram.

Table 3. Iron Heating Response Function in Various Units

Gamma-Ray Group	E_γ(Upper)	H(MeV barns/atom)	H(cm^2 ergs/gram)	H(cm^2/gram)
1	14 MeV	27.47	4.747(-7)*	0.02468
2	10	19.18	3.314(-7)	0.02297
3	8	15.24	2.633(-7)	0.02190
4	7	12.91	2.231(-7)	0.02141
5	6	10.77	1.861(-7)	0.02111
6	5	8.736	1.510(-7)	0.02093
7	4	6.795	1.174(-7)	0.02093
8	3	5.070	8.761(-8)	0.02186
9	2	3.760	6.497(-8)	0.02316
10	1.5	2.904	5.018(-8)	0.02504
11	1	2.243	3.876(-8)	0.02687
12	0.8	1.928	3.332(-8)	0.02771
13	0.7	1.708	2.951(-8)	0.02833
14	0.6	1.368	2.364(-8)	0.02949
15	0.4	0.9777	1.689(-8)	0.03513
16	0.2	1.234	2.132(-8)	0.08868
17	0.1	3.256	5.626(-8)	0.4387
18	0.06	10.71	1.851(-7)	2.566
19	0.03	31.49	5.441(-7)	13.58
20	0.02	86.17	1.489(-6)	61.93
	0.01			

*Read 4.747 x 10^{-7}, etc.

The Prompt-Fission Gammay-Ray Source

A definitive reference to the description of the prompt ($<5\times10^{-8}$ sec after fission) gamma-ray source is the work of Maienschein and Peelle described in a review article by Maienschein (6). The absolute spectrum used in these calculations is given in Table 4. In the region between 1 and 8 MeV it is based on the recommended empirical relationship $N(E)=8.0\exp(-1.1E)$ in photons/fission/MeV, with E in MeV.

Table 4. Absolute Spectrum of Prompt Gamma Rays in Photons per Fission

Gamma-Ray Group	Eγ (Upper)	Source
1	14 MeV	---
2	10	0.0002
3	8	0.0022
4	7	0.0066
5	6	0.020
6	5	0.060
7	4	0.18
8	3	0.54
9	2	0.59
10	1.5	1.00
11	1	0.68
12	0.8	0.50
13	0.7	0.60
14	0.6	1.8
15	0.4	2.7
16	0.2	1.2
17-20	0.2	---
	0.01	
TOTALS		9.88

Since the VENTURE sources input to DOT are in units of neutron densities per sec, the source of prompt gamma rays appearing in Table 4 must be divided by $\bar{\nu}$, the number of neutrons per fission averaged over the thermal neutron spectrum, when the contribution from this component is calculated in a gamma-only problem.

The Fission-Product Gamma-Ray Source

At first glance the representation of the complicated time behavior of both the intensity and spectrum of gamma-ray sources arising from isomeric transitions or following beta decay of the fission products formed after fission represents a formidable problem, which among other things depends on the past irradiation history of each element present in the core. Fortunately, the intensity of such gamma rays decreases rapidly after the fission event, so that about 75% of all fission-product gamma radiation is emitted within about 15 minutes (7). Thus an operating reactor quickly approaches an equilibrium gamma-ray source, and past irradiations and long term beta decays do not contribute to the establishment of this equilibrium.

An updated fission-product gamma-ray source file as a function of energy (22 groups in the range 0-7.5 MeV) and time after fission (0.1 sec to 1.0×10^9 sec) following thermal fission of ^{235}U is available in a Los Alamos report (8). By using parameter fits supplied in this report to each gamma group, it is a simple matter of integrating the semi-empirical exponential expressions, in units of photons per fission per second, over a time interval equivalent to the middle-of-cycle irradiation time of the startup experiment (~9 days), which is the average time after fission a typical gamma-ray may contribute to the equilibrium source (this source is very insensitive to the upper limit cutoff). Thus

$$S_g(E_g,T) = \int_{T_\ell}^{T_u} \sum_{i=1}^{n} \alpha_i e^{-\lambda_i t} dt = \sum_{i=1}^{n} \frac{\alpha_i}{\lambda_i} \left[e^{-\lambda_i T_\ell} - e^{-\lambda_i T_u} \right] , \qquad (5)$$

where $S_g(E_g,T)$ is in units of photons per fission in gamma group g and the parameters α_i and λ_i are functions of g. T_u is 9 days and T_ℓ is 0.1 sec (n is also a function of g, varying between 10 and 16). $S_g(E_g,T)$ in Eq. (5) also represents the approximate equilibrium production rate per fission per second at any instant of time about 15 minutes after constant reactor power is attained. (The time scale can be interpreted both as time after a given fission event or as the time distribution of fission events.)

Table 5 presents the results of regrouping the results of Eq. (5) into the SAILOR group structure. As in the case of the prompt source, the fission in a gamma-ray product source must be divided by $\bar{\nu}$ when the contribution from this component is calculated.

Comparison of Tables 4 and 5 shows the two gamma spectra are very similar, but with the magnitude of the fission-product component about 70% of the prompt component. Both the total fission-product gamma production and the average energy release per fission extracted from Table 5 fall within 10% of the values estimated in 1968 by Maienschein (7). The contributions from ^{239}Pu and ^{238}U have been neglected in this analysis because of the highly enriched (~93%) fuel used in the ORR core.

Table 5. Absolute Spectrum of Equilibrium Fission-Product Gamma Rays in Photons per Fission

Gamma-Ray Group	E_γ (Upper)	Source
1	14 MeV	---
2	10	---
3	8	0.00025
4	7	0.00050
5	6	0.0069
6	5	0.0389
7	4	0.0417
8	3	0.341
9	2	0.336
10	1.5	1.10
11	1	0.788
12	0.8	0.475
13	0.7	0.647
14	0.6	1.14
15	0.4	1.14
16	0.2	0.705
17	0.1	0.108
18	0.06	0.0808
19	0.03	0.0269
20	0.02	0.0269
	0.01	
TOTALS		7.00

Normalization of the Transport Calculations

The neutron and gamma-ray source strengths integrated over the ORR core are the following. For neutrons,

$$S_n = 7.71 \times 10^{16} \text{ neuts/MWt} \times 30 \text{ MWt} = 2.31 \times 10^{18} \text{ neutrons per sec;}$$

for the prompt gamma rays,

$$S_p = 2.31 \times 10^{18} \text{ neutrons/sec} \times \frac{1}{2.42} \text{ fissions/neutron} \times$$

$$\times 9.88 \text{ photons/fission} = 9.43 \times 10^{18} \text{ photons per sec;}$$

and for the fission-product gamma rays,

$$S_{fp} = 2.31 \times 10^{18} \text{ neutrons/sec} \times \frac{1}{2.42} \text{ fissions/neutron} \times$$

$$\times 7.00 \text{ photons/fission} = 6.68 \times 10^{18} \text{ photons per sec.}$$

Table 6 illustrates the normalization of each of the nine transport calculations performed, together with some details of each calculation. In Table 6, it is to be observed tnat each particular geometry (such as XY, etc.) uses the same spatial source distribution but different energy distributions. XNF in both DOT and ANISN is the value to which the source is normalized, and an integration factor IF is also listed which represents a multiplication factor that changes the average calculated fluxes to integrals over the unused dimensions (such as Z, etc.). The product of XNF and IF represents the total number of source particles in the ORR core and should agree with the three values presented at the beginning of this section.

Results and Discussion

The fluxes obtained from each of the nine transport calculations identified in Table 6 having been incorporated into the three-dimensional flux synthesis prescription presented earlier in Eq. (1), the three components of the gamma-ray field may be obtained for the startup experiment as

$$[\phi_g(x,y,z)]_{prompt}, \quad [\phi_g(x,y,z)]_{fission\text{-}product}, \quad \text{and} \quad \{[\phi_g(x,y,z)]_{prompt + non\text{-}fission} - [\phi_g(x,y,z)]_{prompt}\},$$

where the difference spectra in the third expression represents the non-fission component. One advantage of using the average fluxes is their near-constant magnitude regardless of geometry, i.e., $\phi_g(x,y)$, $\phi_g(y,z)$, and $\phi_g(y)$ all lie within 10% or so of each other at locations near the y-axis. Consequently, values of $\phi_g(0,y,0)$ may be accurately estimated using the $\phi_g(0,y)$ values in the XY calculation only, although this approximation was not employed in the present results. The close equivalence of the near-centerline flux averaged over the axial direction and the near-centerline flux near the midplane is a consequence of the slowly varying flux profile with axial location. A similar equivalence exists for the crosswise dimension. This approximation becomes worse with increasing y. (See Tables 7-12).

Table 6. Normalization and Other Source Details for the Transport Calculations

GEOMETRY	Source Distributions: Spatial	Source Distributions: Energy	XNF	IF	^{235}U conc.	Type
		Neutrons + Prompts + All Non-Fission Gamma Rays				
XY	Z-integrated VENTURE source	χ for neutrons	3.88(16)*	60.96	Z-averaged	coupled
YZ	X-integrated VENTURE source	and 0 for gammas	4.33(16)	53.34	X-averaged	coupled
Y	X- and Z-integrated VENTURE source		7.10(14)	53.34 x 60.96	X- and Z-averaged	coupled
		Prompt Gamma-Rays				
XY	Z-integrated VENTURE source	0 for neutrons	1.55(17)	60.96	Z-averaged	gamma only
YZ	X-integrated VENTURE source	Table 4 divided	1.77(17)	53.34	X-averaged	gamma only
Y	X- and Z-integrated VENTURE source	by 2.42 for gammas	2.90(15)	53.34 x 60.96	X- and Z-averaged	gamma only
		Fission-Product Gamma-Rays				
XY	Z-integrated VENTURE source	0 for neutrons	1.10(17)	60.96	Z-averaged	gamma only
YZ	X-integrated VENTURE source	Table 5 divided	1.25(17)	53.34	X-averaged	gamma only
Y	X- and Z-integrated VENTURE source	by 2.42 for gammas	2.05(15)	53.34 x 60.96	X- and Z-averaged	gamma only

*Read 3.88×10^{16}. This value has been increased by 2.3% to absorb the bias factor accounting for enhanced neutron transmission through the heterogeneous plate and water fuel element geometry in the ORR core that was homogenized in this calculation. No such bias factor was used to correct for any differences in gamma-ray transmission.

Table 7. Average Gamma-Ray Fluxes at the Center of the SSC-1* During the Two-Year Experiment in Units of Photons/cm^2/sec

	Prompt				Fission-Product				Non-Fission				Total
IG†	ϕ_{XY}	ϕ_{YZ}	ϕ_{Y}	ϕ_{XYZ}	ϕ_{XY}	ϕ_{YZ}	ϕ_{Y}	ϕ_{XYZ}	ϕ_{XY}	ϕ_{YZ}	ϕ_{Y}	ϕ_{XYZ}	ϕ_{XYZ}
2	3.07(8)*	3.64(8)	3.59(8)	3.11(8)	0	0	0	0	3.72(11)	3.72(11)	3.37(11)	4.11(11)	4.11(11)
3	3.33(9)	3.94(9)	3.87(9)	3.39(9)	3.78(8)	4.42(8)	4.34(8)	3.85(8)	1.53(12)	1.55(12)	1.44(12)	1.64(12)	1.64(12)
4	9.48(9)	1.12(10)	1.09(10)	9.72(9)	6.79(8)	7.93(8)	7.74(8)	6.95(8)	4.30(11)	4.38(11)	4.13(11)	4.56(11)	4.66(11)
5	2.80(10)	3.29(10)	3.19(10)	2.88(10)	9.04(9)	1.05(10)	1.02(10)	9.39(9)	5.31(11)	5.45(11)	5.21(11)	5.55(11)	5.93(11)
6	7.48(10)	8.74(10)	8.41(10)	7.79(10)	4.50(10)	5.21(10)	4.97(10)	4.71(10)	6.59(11)	6.81(11)	6.61(11)	6.79(11)	8.04(11)
7	1.95(11)	2.27(11)	2.16(11)	2.05(11)	5.71(10)	6.58(10)	6.33(10)	5.93(10)	8.59(11)	8.89(11)	8.79(11)	8.69(11)	1.13(12)
8	4.40(11)	5.06(11)	4.73(11)	4.71(11)	2.38(11)	2.71(11)	2.51(11)	2.58(11)	1.80(12)	1.85(12)	1.84(12)	1.81(12)	2.54(12)
9	4.37(11)	4.98(11)	4.63(11)	4.71(11)	2.38(11)	2.68(11)	2.48(11)	2.58(11)	1.18(12)	1.21(12)	1.23(12)	1.16(12)	1.89(12)
10	7.13(11)	8.05(11)	7.46(11)	7.69(11)	4.90(11)	5.47(11)	4.97(11)	5.39(11)	1.59(12)	1.64(12)	1.68(12)	1.55(12)	2.86(12)
11	4.25(11)	4.77(11)	4.42(11)	4.60(11)	3.10(11)	3.44(11)	3.11(11)	3.43(11)	1.52(12)	1.55(12)	1.52(12)	1.55(12)	2.35(12)
12	2.67(11)	2.99(11)	2.76(11)	2.89(11)	1.97(11)	2.18(11)	1.97(11)	2.18(11)	6.16(11)	6.34(11)	6.45(11)	6.05(11)	1.11(12)
13	3.23(11)	3.61(11)	3.33(11)	3.50(11)	2.43(11)	2.67(11)	2.41(11)	2.69(11)	7.38(11)	7.59(11)	7.73(11)	7.25(11)	1.32(12)
14	1.07(12)	1.19(12)	1.10(12)	1.15(12)	7.63(11)	8.37(11)	7.59(11)	8.40(11)	3.57(12)	3.66(12)	3.65(12)	3.58(12)	5.57(12)
15	1.93(12)	2.15(12)	1.99(12)	2.09(12)	1.39(12)	1.52(12)	1.38(12)	1.53(12)	5.43(12)	5.57(12)	5.60(12)	5.40(12)	9.02(12)
16	1.18(12)	1.31(12)	1.20(12)	1.29(12)	8.50(11)	9.28(11)	8.35(11)	9.39(11)	3.37(12)	3.45(12)	3.46(12)	3.36(12)	5.59(12)
17	9.09(10)	1.00(11)	9.25(10)	9.81(10)	6.54(10)	7.09(10)	6.42(10)	7.22(10)	2.61(11)	2.64(11)	2.65(11)	2.60(11)	4.30(11)
18	4.67(8)	5.19(8)	4.78(8)	5.08(8)	3.36(8)	3.67(8)	3.31(8)	3.72(8)	9.06(9)	8.97(9)	8.48(9)	9.58(9)	1.05(10)
19	3.40(4)	3.79(4)	3.49(4)	3.69(4)	2.45(4)	2.68(4)	2.42(4)	2.71(4)	4.71(8)	4.65(8)	4.37(8)	5.01(8)	5.01(8)
20	6.86(0)	7.65(0)	7.06(0)	7.47(0)	4.93(0)	5.41(0)	4.90(0)	5.45(0)	9.75(7)	9.77(7)	9.05(7)	1.05(8)	1.05(8)

*Actual location is 13.3cm from the outside surface of the aluminum window, along the radial centerline, and 5.35cm below the horizontal reactor midplane.

†See Tables 4 or 5 for the gamma-ray group boundaries.

*Read 3.07 x 10^8, etc.

Table 8. Average Gamma-Ray Fluxes at the Center of the SSC-2* During the Two-Year Experiment in Units of Photons/cm^2/sec

IG†	Prompt				Fission-Product				Non-Fission				Total
	ϕ_{XY}	ϕ_{YZ}	ϕ_{Y}	ϕ_{XYZ}	ϕ_{XY}	ϕ_{YZ}	ϕ_{Y}	ϕ_{XYZ}	ϕ_{XY}	ϕ_{YZ}	ϕ_{Y}	ϕ_{XYZ}	ϕ_{XYZ}
2	3.56(8)‡	4.22(8)	4.16(8)	3.61(8)	0	0	0	0	4.32(11)	4.32(11)	3.91(11)	4.77(11)	4.77(11)
3	3.86(9)	4.57(9)	4.49(9)	3.93(9)	4.38(8)	5.13(8)	5.03(8)	4.47(8)	1.78(12)	1.80(12)	1.67(12)	1.90(12)	1.90(12)
4	1.10(10)	1.29(10)	1.26(10)	1.13(10)	7.88(8)	9.19(8)	8.98(8)	8.06(8)	4.99(11)	5.08(11)	4.79(11)	5.29(11)	5.41(11)
5	3.25(10)	3.82(10)	3.70(10)	3.35(10)	1.05(10)	1.22(10)	1.18(10)	1.09(10)	6.16(11)	6.32(11)	6.05(11)	6.44(11)	6.88(11)
6	8.68(10)	1.01(11)	9.75(10)	9.03(10)	5.22(10)	6.04(10)	5.77(10)	5.47(10)	7.65(11)	7.90(11)	7.67(11)	7.88(11)	9.33(11)
7	2.27(11)	2.63(11)	2.50(11)	2.38(11)	6.63(10)	7.63(10)	7.35(10)	6.88(10)	9.97(11)	1.03(12)	1.02(12)	1.02(12)	1.32(12)
8	5.11(11)	5.86(11)	5.48(11)	5.47(11)	2.77(11)	3.14(11)	2.91(11)	2.99(11)	2.09(12)	2.15(12)	2.14(12)	2.10(12)	2.95(12)
9	5.07(11)	5.77(11)	5.37(11)	5.46(11)	2.76(11)	3.11(11)	2.88(11)	2.98(11)	1.37(12)	1.40(12)	1.42(12)	1.35(12)	2.20(12)
10	8.27(11)	9.33(11)	8.66(11)	8.91(11)	5.69(11)	6.34(11)	5.77(11)	6.25(11)	1.84(12)	1.90(12)	1.95(12)	1.79(12)	3.31(12)
11	4.93(11)	5.54(11)	5.12(11)	5.33(11)	3.60(11)	3.99(11)	3.61(11)	3.98(11)	1.76(12)	1.80(12)	1.76(12)	1.80(12)	2.73(12)
12	3.10(11)	3.47(11)	3.20(11)	3.36(11)	2.29(11)	2.52(11)	2.28(11)	2.53(11)	7.15(11)	7.36(11)	7.47(11)	7.02(11)	1.29(12)
13	3.75(11)	4.19(11)	3.87(11)	4.06(11)	2.81(11)	3.09(11)	2.80(11)	3.11(11)	8.56(11)	8.81(11)	8.96(11)	8.41(11)	1.53(12)
14	1.24(12)	1.38(12)	1.28(12)	1.34(12)	8.85(11)	9.71(11)	8.81(11)	9.75(11)	4.14(12)	4.25(12)	4.23(12)	4.16(12)	6.46(12)
15	2.24(12)	2.50(12)	2.31(12)	2.43(12)	1.62(12)	1.77(12)	1.60(12)	1.79(12)	6.30(12)	6.46(12)	6.50(12)	6.26(12)	1.05(13)
16	1.37(12)	1.52(12)	1.40(12)	1.49(12)	9.86(11)	1.08(12)	9.69(11)	1.09(12)	3.91(12)	4.00(12)	4.01(12)	3.90(12)	6.49(12)
17	1.05(11)	1.16(11)	1.07(11)	1.14(11)	7.59(10)	8.22(10)	7.45(10)	8.37(10)	3.03(11)	3.06(11)	3.08(11)	3.01(11)	4.99(11)
18	5.42(8)	6.02(8)	5.54(8)	5.89(8)	3.90(8)	4.25(8)	3.85(8)	4.31(8)	1.05(10)	1.04(10)	9.85(9)	1.11(10)	1.22(10)
19	3.95(4)	4.40(4)	4.05(4)	4.29(4)	2.84(4)	3.11(4)	2.81(4)	3.15(4)	5.46(8)	5.39(8)	5.07(8)	5.80(8)	5.80(8)
20	7.96(0)	8.87(0)	8.19(0)	8.62(0)	5.72(0)	6.27(0)	5.68(0)	6.32(0)	1.13(8)	1.13(8)	1.05(8)	1.22(8)	1.22(8)

*Same location as in the SSC-1.

†See Tables 4 or 5 for the gamma-ray group boundaries.

‡Read 3.56 x 10^8, etc.

Table 9. Average Gamma-Ray Fluxes at the "OT" Location in the SPVC* During the Two-Year Experiment in Units of Photons/cm^2/sec

IG†	Prompt				Fission-Product				Non-Fission				Total
	ϕ_{XY}	ϕ_{YZ}	ϕ_{Y}	ϕ_{XYZ}	ϕ_{XY}	ϕ_{YZ}	ϕ_{Y}	ϕ_{XYZ}	ϕ_{XY}	ϕ_{YZ}	ϕ_{Y}	ϕ_{XYZ}	ϕ_{XYZ}
2	6.75(7)‡	8.26(7)	8.77(7)	6.37(7)	0	0	0	0	1.20(11)	1.19(11)	1.22(11)	1.17(11)	1.17(11)
3	7.28(8)	8.89(8)	9.39(8)	6.89(8)	8.21(7)	9.93(7)	1.05(8)	7.76(7)	6.28(11)	6.51(11)	6.47(11)	6.32(11)	6.33(11)
4	2.04(9)	2.49(9)	2.62(9)	1.94(9)	1.48(8)	1.78(8)	1.88(8)	1.40(8)	1.66(11)	1.72(11)	1.75(11)	1.63(11)	1.65(11)
5	5.99(9)	7.24(9)	7.58(9)	5.72(9)	1.88(9)	2.26(9)	2.35(9)	1.80(9)	2.02(11)	2.11(11)	2.15(11)	1.98(11)	2.06(11)
6	1.54(10)	1.85(10)	1.92(10)	1.48(10)	1.96(9)	1.07(10)	1.10(10)	3.72(9)	2.44(11)	2.57(11)	2.63(11)	2.38(11)	2.62(11)
7	3.86(10)	4.59(10)	4.72(10)	3.76(10)	1.20(10)	1.41(10)	1.46(10)	1.16(10)	3.04(11)	3.20(11)	3.33(11)	2.92(11)	3.41(11)
8	8.05(10)	9.41(10)	9.52(10)	7.95(10)	4.12(10)	4.78(10)	4.78(10)	4.12(10)	7.27(11)	7.67(11)	7.86(11)	7.09(11)	8.30(11)
9	7.74(10)	8.95(10)	8.99(10)	7.70(10)	4.07(10)	4.66(10)	4.64(10)	4.09(10)	4.19(11)	4.40(11)	4.57(11)	4.03(11)	5.21(11)
10	1.22(11)	1.39(11)	1.39(11)	1.22(11)	7.47(10)	8.45(10)	8.30(10)	7.61(10)	5.18(11)	5.47(11)	5.75(11)	4.93(11)	6.91(11)
11	7.02(10)	8.00(10)	7.96(10)	7.06(10)	4.50(10)	5.06(10)	4.93(10)	4.62(10)	3.90(11)	4.09(11)	4.22(11)	3.78(11)	4.95(11)
12	4.31(10)	4.89(10)	4.85(10)	4.35(10)	2.79(10)	3.13(10)	3.04(10)	2.87(10)	1.86(11)	1.95(11)	2.05(11)	1.76(11)	2.48(11)
13	5.13(10)	5.82(10)	5.76(10)	5.19(10)	3.35(10)	3.75(10)	3.64(10)	3.45(10)	2.33(11)	2.45(11)	2.56(11)	2.23(11)	3.10(11)
14	1.67(11)	1.90(11)	1.88(11)	1.69(11)	1.05(11)	1.17(11)	1.14(11)	1.08(11)	1.21(12)	1.27(12)	1.32(12)	1.16(12)	1.44(12)
15	2.97(11)	3.39(11)	3.33(11)	3.03(11)	1.89(11)	2.12(11)	2.04(11)	1.97(11)	1.79(12)	1.88(12)	1.96(12)	1.71(12)	2.21(12)
16	1.84(11)	2.10(11)	2.05(11)	1.89(11)	1.17(11)	1.32(11)	1.26(11)	1.23(11)	1.13(12)	1.18(12)	1.23(12)	1.08(12)	1.39(12)
17	1.44(10)	1.66(10)	1.62(10)	1.48(10)	9.20(9)	1.05(10)	9.94(9)	9.70(9)	8.81(10)	9.31(10)	9.65(10)	8.50(10)	1.10(11)
18	7.82(7)	9.09(7)	8.42(7)	8.45(7)	4.99(7)	5.72(7)	5.17(7)	5.52(7)	3.60(9)	3.73(9)	3.68(9)	3.65(9)	3.79(9)
19	5.77(3)	6.69(3)	6.22(3)	6.21(3)	3.68(3)	4.21(3)	3.82(3)	4.06(3)	1.91(8)	1.96(8)	1.91(8)	1.96(8)	1.96(8)
20	1.17(0)	1.35(0)	1.26(0)	1.26(0)	7.45(-1)	8.51(-1)	7.72(-1)	8.21(-1)	3.95(7)	4.05(7)	3.93(7)	4.07(7)	4.07(7)

*Actual locations 22.39cm from the outside surface of the aluminum window (i.e., 2.42cm inside the SPVC), along the radial centerline, and 5.35cm below the horizontal reactor midplane.

†See Tables 4 or 5 for the gamma-ray group boundaries.

‡Read 6.75 x 10^7, etc.

Table 10. Average Gamma-Ray Fluxes at the T/4 Location in the SPVC* During the Two-Year Experiment in Units of Photons/cm^2/sec

IG†	Prompt				Fission-Product				Non-Fission				Total
	ϕ_{XY}	ϕ_{YZ}	ϕ_{Y}	ϕ_{XYZ}	ϕ_{XY}	ϕ_{YZ}	ϕ_{Y}	ϕ_{XYZ}	ϕ_{XY}	ϕ_{YZ}	ϕ_{Y}	ϕ_{XYZ}	ϕ_{XYZ}
2	2.33(7)‡	2.84(7)	3.00(7)	2.21(7)	0	0	0	0	3.32(10)	3.42(10)	3.40(10)	3.34(10)	3.34(10)
3	2.52(8)	3.07(8)	3.23(8)	2.40(8)	2.84(7)	3.42(7)	3.59(7)	2.71(7)	1.73(11)	1.81(11)	1.84(11)	1.70(11)	1.70(11)
4	7.10(8)	8.59(8)	9.00(8)	6.78(8)	5.17(7)	6.20(7)	6.51(7)	4.92(7)	5.27(10)	5.55(10)	5.69(10)	5.14(10)	5.21(10)
5	2.07(9)	2.49(9)	2.60(9)	1.98(9)	6.38(8)	7.63(8)	7.91(8)	6.15(8)	6.47(10)	6.78(10)	7.00(10)	6.27(10)	6.53(10)
6	5.21(9)	6.23(9)	6.45(9)	5.03(9)	2.97(9)	3.52(9)	3.62(9)	2.89(9)	7.99(10)	8.13(10)	8.47(10)	7.67(10)	8.46(10)
7	1.28(10)	1.52(10)	1.56(10)	1.25(10)	4.12(9)	4.82(9)	5.01(9)	3.96(9)	1.04(11)	1.05(11)	1.11(11)	9.80(10)	1.15(11)
8	2.56(10)	2.99(10)	3.03(10)	2.53(10)	1.27(10)	1.47(10)	1.47(10)	1.27(10)	2.04(11)	2.02(11)	2.09(11)	1.97(11)	2.35(11)
9	2.39(10)	2.76(10)	2.79(10)	2.36(10)	1.22(10)	1.40(10)	1.40(10)	1.22(10)	1.39(11)	1.33(11)	1.40(11)	1.32(11)	1.68(11)
10	3.65(10)	4.19(10)	4.21(10)	3.63(10)	2.10(10)	2.38(10)	2.35(10)	2.13(10)	1.85(11)	1.73(11)	1.83(11)	1.75(11)	2.33(11)
11	2.06(10)	2.36(10)	2.36(10)	2.06(10)	1.22(10)	1.38(10)	1.36(10)	1.24(10)	1.56(11)	1.51(11)	1.56(11)	1.51(11)	1.84(11)
12	1.25(10)	1.43(10)	1.43(10)	1.25(10)	7.46(9)	8.42(9)	8.26(9)	7.60(9)	6.95(10)	6.51(10)	6.86(10)	6.60(10)	8.61(10)
13	1.47(10)	1.68(10)	1.68(10)	1.47(10)	8.84(9)	9.96(9)	9.77(9)	9.01(9)	8.24(10)	7.71(10)	8.13(10)	7.81(10)	1.02(11)
14	4.84(10)	5.54(10)	5.55(10)	4.83(10)	2.78(10)	3.14(10)	3.09(10)	2.82(10)	4.20(11)	4.12(11)	4.29(11)	4.03(11)	4.80(11)
15	8.40(10)	9.60(10)	9.61(10)	8.39(10)	4.90(10)	5.52(10)	5.42(10)	4.99(10)	6.26(11)	6.06(11)	6.33(11)	5.99(11)	7.33(11)
16	5.09(10)	5.82(10)	5.84(10)	5.07(10)	2.97(10)	3.35(10)	3.30(10)	3.02(10)	3.87(11)	3.74(11)	3.92(11)	3.69(11)	4.50(11)
17	4.05(9)	4.67(9)	4.65(9)	4.07(9)	2.37(9)	2.69(9)	2.63(9)	2.42(9)	3.07(10)	2.99(10)	3.12(10)	2.94(10)	3.59(10)
18	2.14(7)	2.48(7)	2.57(7)	2.07(7)	1.25(7)	1.43(7)	1.45(7)	1.23(7)	6.16(8)	6.27(8)	6.40(8)	6.03(8)	6.37(8)
19	1.57(3)	1.81(3)	1.87(3)	1.52(3)	9.16(2)	1.04(3)	1.06(3)	8.5[illegible](2)	2.47(7)	2.53(7)	2.60(7)	2.40(7)	2.40(7)
20	3.16(-1)	3.64(-1)	3.77(-1)	3.05(-1)	1.85(-1)	2.10(-1)	2.13(-1)	1.82(-1)	5.02(6)	5.14(6)	5.28(6)	4.89(6)	4.89(6)

*Actual location is 28.38cm from the outside surface of the aluminum window (i.e., 6.41cm inside the SPVC), along the radial centerline, and 5.35cm below the horizontal reactor midplane.

†See Tables 4 or 5 for the gamma-ray group boundaries.

‡Read 2.33 x 10^7, etc.

Table 11. Average Gamma-Ray Fluxes at the T/2 Location in the SPVC* During the Two-Year Experiment in Units of Photons/cm^2/sec

IG†	Prompt				Fission-Product				Non-Fission				Total
	ϕ_{XY}	ϕ_{YZ}	ϕ_{Y}	ϕ_{XYZ}	ϕ_{XY}	ϕ_{YZ}	ϕ_{Y}	ϕ_{XYZ}	ϕ_{XY}	ϕ_{YZ}	ϕ_{Y}	ϕ_{XYZ}	ϕ_{XYZ}
2	6.15(6)‡	7.40(6)	7.80(6)	5.83(6)	0	0	0	0	8.28(9)	8.59(9)	8.77(9)	8.11(9)	8.12(9)
3	6.69(7)	8.03(7)	8.43(7)	6.37(7)	7.50(6)	8.92(6)	9.35(6)	7.16(6)	4.28(10)	4.51(10)	4.86(10)	3.97(10)	3.98(10)
4	1.88(8)	2.25(8)	2.35(8)	1.80(8)	1.38(7)	1.64(7)	1.72(7)	1.32(7)	1.47(10)	1.55(10)	1.66(10)	1.38(10)	1.40(10)
5	5.45(8)	6.49(8)	6.77(8)	5.22(8)	1.64(8)	1.94(8)	2.01(8)	1.58(8)	1.81(10)	1.93(10)	2.07(10)	1.69(10)	1.76(10)
6	1.34(9)	1.59(9)	1.64(9)	1.30(9)	7.42(8)	8.72(8)	8.95(8)	7.23(8)	2.26(10)	2.41(10)	2.61(10)	2.09(10)	2.29(10)
7	3.21(9)	3.76(9)	3.87(9)	3.12(9)	1.07(9)	1.24(9)	1.29(9)	1.03(9)	3.02(10)	3.23(10)	3.50(10)	2.79(10)	3.21(10)
8	6.08(9)	7.06(9)	7.19(9)	5.97(9)	2.89(9)	3.33(9)	3.35(9)	2.87(9)	5.17(10)	5.53(10)	5.92(10)	4.83(10)	5.71(10)
9	5.46(9)	6.30(9)	6.39(9)	5.38(9)	2.69(9)	3.08(9)	3.10(9)	2.67(9)	3.80(10)	4.06(10)	4.37(10)	3.53(10)	4.34(10)
10	8.07(9)	9.28(9)	9.38(9)	7.98(9)	4.30(9)	4.90(9)	4.88(9)	4.32(9)	5.22(10)	5.58(10)	5.99(10)	4.86(10)	6.09(10)
11	4.47(9)	5.14(9)	5.19(9)	4.43(9)	2.43(9)	2.76(9)	2.75(9)	2.44(9)	5.30(10)	5.63(10)	5.88(10)	5.07(10)	5.76(10)
12	2.68(9)	3.08(9)	3.11(9)	2.65(9)	1.47(9)	1.67(9)	1.65(9)	1.49(9)	2.08(10)	2.22(10)	2.35(10)	1.96(10)	2.37(10)
13	3.14(9)	3.60(9)	3.64(9)	3.11(9)	1.72(9)	1.95(9)	1.94(9)	1.73(9)	2.40(10)	2.56(10)	2.73(10)	2.25(10)	2.73(10)
14	1.05(10)	1.21(10)	1.22(10)	1.04(10)	5.51(9)	6.25(9)	6.24(9)	5.52(9)	1.16(11)	1.23(11)	1.31(11)	1.09(11)	1.25(11)
15	1.81(10)	2.07(10)	2.10(10)	1.78(10)	9.62(9)	1.09(10)	1.09(10)	9.62(9)	1.75(11)	1.86(11)	1.99(11)	1.64(11)	1.91(11)
16	1.09(10)	1.25(10)	1.27(10)	1.07(10)	5.83(9)	6.59(9)	6.59(9)	5.83(9)	1.08(11)	1.15(11)	1.23(11)	1.01(11)	1.18(11)
17	8.69(8)	1.01(9)	1.01(9)	8.05(8)	4.64(8)	5.30(8)	5.24(8)	4.69(8)	8.54(9)	9.13(9)	9.74(9)	8.01(9)	9.28(9)
18	4.61(6)	5.33(6)	5.57(6)	4.41(6)	2.47(6)	2.80(6)	2.89(6)	2.39(6)	1.60(8)	1.68(8)	1.88(8)	1.43(8)	1.50(8)
19	3.37(2)	3.88(2)	4.05(2)	3.23(2)	1.80(2)	2.04(2)	2.10(2)	1.75(2)	6.29(6)	6.49(6)	7.49(6)	5.45(6)	5.45(6)
20	6.80(-2)	7.83(-2)	8.17(-2)	6.52(-2)	3.64(-2)	4.12(-2)	4.24(-2)	3.54(-2)	1.28(6)	1.32(6)	1.53(6)	1.10(6)	1.10(6)

*Actual location is 33.52cm from the outside surface of the aluminum window (i.e., 11.55cm inside the SPVC), along the radial centerline and 5.35cm below the horizontal reactor midplane.

†See Tables 4 or 5 for the gamma-ray group boundaries.

‡Read 6.15 x 10^6, etc.

Table 12. Average Gamma-Ray Fluxes at the 3T/4 Location in the SPVC* During the Two-Year Experiment in Units of Photons/cm^2/sec

IG†	Prompt				Fission-Product				Non-Fission				Total
	ϕ_{XY}	ϕ_{YZ}	ϕ_{Y}	ϕ_{XYZ}	ϕ_{XY}	ϕ_{YZ}	ϕ_{Y}	ϕ_{XYZ}	ϕ_{XY}	ϕ_{YZ}	ϕ_{Y}	ϕ_{XYZ}	ϕ_{XYZ}
2	1.54(6)*	1.83(6)	1.93(6)	1.46(6)	0	0	0	0	4.30(9)	2.98(9)	3.95(9)	3.24(9)	3.24(9)
3	1.68(7)	1.99(7)	2.10(7)	1.59(7)	1.88(6)	2.20(6)	2.32(6)	1.78(6)	1.45(10)	1.62(10)	2.30(10)	1.02(10)	1.02(10)
4	4.73(7)	5.58(7)	5.85(7)	4.51(7)	3.50(6)	4.09(6)	4.30(6)	3.33(6)	5.31(9)	5.47(9)	7.17(9)	4.05(9)	4.10(9)
5	1.36(8)	1.60(8)	1.67(8)	1.30(8)	4.01(7)	4.67(7)	4.86(7)	3.85(7)	6.36(9)	6.66(9)	8.67(9)	4.89(9)	5.06(9)
6	3.25(8)	3.81(8)	3.96(8)	3.13(8)	1.75(8)	2.03(8)	2.09(8)	1.70(8)	7.58(9)	8.34(9)	1.08(10)	5.85(9)	6.33(9)
7	7.55(8)	8.79(8)	9.09(8)	7.30(8)	2.59(8)	2.99(8)	3.12(8)	2.48(8)	1.02(10)	1.11(10)	1.40(10)	8.09(9)	9.07(9)
8	1.36(9)	1.57(9)	1.61(9)	1.33(9)	6.22(8)	7.14(8)	7.25(8)	6.13(8)	1.72(10)	1.85(10)	2.58(10)	1.23(10)	1.42(10)
9	1.18(9)	1.36(9)	1.39(9)	1.15(9)	5.61(8)	6.43(8)	6.49(8)	5.56(8)	1.25(10)	1.33(10)	1.75(10)	9.50(9)	1.12(10)
10	1.70(9)	1.96(9)	1.99(9)	1.67(9)	8.49(8)	9.72(8)	9.74(8)	8.47(8)	1.69(10)	1.77(10)	2.27(10)	1.32(10)	1.57(10)
11	9.31(8)	1.08(9)	1.09(9)	9.22(8)	4.72(8)	5.39(8)	5.39(8)	4.72(8)	1.80(10)	2.05(10)	2.37(10)	1.56(10)	1.70(10)
12	5.56(8)	6.43(8)	6.50(8)	5.50(8)	2.83(8)	3.23(8)	3.23(8)	2.83(8)	6.89(9)	7.30(9)	8.94(9)	5.63(9)	6.46(9)
13	6.49(8)	7.49(8)	7.59(8)	6.40(8)	3.30(8)	3.77(8)	3.77(8)	3.30(8)	7.97(9)	8.50(9)	1.07(10)	6.33(9)	7.30(9)
14	2.21(9)	2.56(9)	2.60(9)	2.18(9)	1.08(9)	1.23(9)	1.24(9)	1.07(9)	3.90(10)	4.10(10)	5.31(10)	3.01(10)	3.34(10)
15	3.77(9)	4.36(9)	4.42(9)	3.72(9)	1.87(9)	2.14(9)	2.14(9)	1.87(9)	5.87(10)	6.20(10)	7.95(10)	4.58(10)	5.14(10)
16	2.30(9)	2.65(9)	2.68(9)	2.27(9)	1.13(9)	1.29(9)	1.29(9)	1.13(9)	3.68(10)	3.84(10)	4.93(10)	2.87(10)	3.21(10)
17	1.82(8)	2.07(8)	2.10(8)	1.79(8)	8.98(7)	1.01(8)	1.01(8)	8.98(7)	2.93(9)	3.01(9)	3.85(9)	2.29(9)	2.56(9)
18	1.01(6)	1.13(6)	1.11(6)	1.03(6)	4.99(5)	5.55(5)	5.36(5)	5.17(5)	5.65(7)	7.47(7)	1.16(8)	3.64(7)	3.80(7)
19	7.56(1)	8.33(1)	8.19(1)	7.69(1)	3.75(1)	4.08(1)	3.95(1)	3.87(1)	2.37(6)	3.56(6)	5.75(6)	1.47(6)	1.47(6)
20	1.55(-2)	1.68(-2)	1.66(-2)	1.57(-2)	7.70(-3)	8.24(-3)	7.98(-3)	7.95(-3)	4.78(5)	7.30(5)	1.18(6)	2.96(5)	2.96(5)

*Actual location is 38.98cm from the outside surface of the aluminum window (i.e., 17.01cm inside the SPVC), along the radial centerline and 5.35cm below the horizontal reactor midplane.

†See Tables 4 or 5 for the gamma-ray group boundaries.

*Read 1.54 x 10^6, etc.

In order to convert gamma-ray flux levels from the startup to the two-year blind test experiments, the relative calculated neutron flux levels in the two experiments must be obtained for each of the three exposures in the two-year experiment. Since the spectral shape of the leakage neutrons was shown to be virtually independent of cycle and the relative intensity independent of detector location (1), it is sufficient to weight a calculated dosimeter saturated activity with the actual power and operating time a cycle group was active, average over all cycle groups in a given exposure, and compare the average activity with the one calculated for the startup experiment. Thus, the average leakage relative to that in the startup experiment becomes:

$$\text{Relative Leakage} = \frac{1}{30 \times RR^d} \left[\sum_G RR_G^d \sum_{i=1}^{L(G)} \Delta tup(i) \times \text{Power}(i)\right] / \sum_G \sum_{i=1}^{L(G)} \Delta tup(i),$$

where RR^d and RR_G^d are the saturated activities for the startup experiment and cycle group G in the two-year experiment for dosimeter d respectively, and Δtup and power represent the uptime and power level for each cycle.

From values appearing in Tables 2 and 4 of Ref. (1) and the choice of the $^{54}Fe(n,p)$ dosimeter, the relative leakages become, for the three exposures, 0.843 for the SSC-1, 0.978 for the SSC-2, and 0.907 for the SPVC.

Tables 7-12 present the results of the individual calculations for each of the gamma-ray components at the various detector locations of interest. The observation alluded to earlier in this section concerning the near-independence of the flux components with geometry for near-centerline detectors located relatively close to the reactor can easily be verified by scanning these tables. Several conclusions can be drawn from these tables. First, the gamma rays arising from non-fission events (i.e., non-fission secondaries produced throughout the configuration) dominate the spectrum. Second, the prompt-fission gamma rays are a factor of 1.5-2 as important as the fission-product component, a conclusion that could have been deduced from their relative source strengths and spectra. Third, the low-energy gamma-ray component below 0.06 MeV (i.e., groups 18-20) is not calculated particularly well because the spatial mesh used in the calculations was too coarse for the extremely short mean free paths at these energies. This is not the reason, however, for the large differences in the low-energy fluxes between the non-fission and fission components. One must infer that the capture gamma-ray spectra include sources in these groups whereas the gamma-ray downscattering matrix used in the transport does not include any transfers into these groups, but instead considers the gammas totally absorbed at some higher energy. This is consistent with the energy absorption response function used in SAILOR which considers fluorescence and bremsstrahlung x-radiation as being

totally absorbed at the place where it is formed. The contribution of the gamma-ray fluxes in groups 18-20 is completely negligible in the heating in the steel, and any error introduced into their calculation should have essentially no effect on the calculated heating rates.

Table 13 presents the relative gamma-ray spectra at each of the five detector locations. An inspection shows these spectra to be closely the same, with only minor differences that are to be expected from the presence of downscattered hydrogen capture gamma rays at the SSC and OT locations and the presence of downscattered stainless steel capture gamma rays formed in the steel layer in contact with the water, also near these same two locations. The largest contributions to the heating rates come from groups 3 (7-8 MeV) and 8 (2-3 MeV), and the peaks in the spectra occur in groups 15 (0.2-0.4 MeV) and 16 (0.1-0.2 MeV), the latter undoubtedly due in part to the slowing down of the 511 keV gamma rays formed from annihilation.

Table 14 presents the results of folding the values of ϕ_{XYZ} for each of the three gamma-ray components in Tables 7-12 with the heating response function tabulated earlier in Table 3. The neutron subcadmium ($E_n \leq 0.414$ eV) fluxes are also presented in Table 14, and it can easily be inferred from the last row that an equilibrium condition has not set in until about a half-thickness depth is penetrated (~12 cm). At shallower penetrations, the thermal neutrons are not as efficient in producing gamma-ray heating because of the small contribution from hydrogen capture relative to that from steel capture.

Table 15 shows the approximate effects of the finite core height on the various gamma-ray components. These "axial leakage factors" were derived as ratios of ϕ_{XYZ} appearing in Tables 7-12 to ϕ_{XY} values renormalized to a midplane source intensity rather than the intensity averaged over the entire height of the core. Thus values in Table 15 were calculated as values of

$$\phi_{XYZ}/(1.34\phi_{XY}) \quad .$$

An examination of Table 15 indicates that the effects of finite source height are essentially independent of detector location for the fission related gamma rays, but tend to be more pronounced with increasing distance from the core for the non-fission gamma rays. Since the latter are presumed to arise as a result of thermal-neutron capture in the vicinity of the detector, these latter leakage factors should be representative of thermal neutron values as well, which they indeed seem to be. The alarming decrease in these latter two factors in going from T/2 to 3T/4 may be due to thermalization of the neutrons in the water beyond the void box and reflection back into the SPVC.*

*The void box was not filled with water in the calculation, even though it was known to have leaked during the course of the two-year irradiation.

Table 13. Relative Total Gamma-Ray Spectra at the Five Detector Locations

IG	E upper	SSC	OT	T/4	T/2	3T/4
2	10 MeV	1.09(-2)	1.17(-2)	1.03(-2)	9.58(-3)	1.41(-2)
3	8	4.35(-2)	6.35(-2)	5.27(-2)	4.69(-2)	4.45(-2)
4	7	1.23(-2)	1.65(-2)	1.61(-2)	1.65(-2)	1.79(-2)
5	6	1.57(-2)	2.07(-2)	2.02(-2)	2.08(-2)	2.21(-2)
6	5	2.13(-2)	2.63(-2)	2.62(-2)	2.70(-2)	2.76(-2)
7	4	3.00(-2)	3.42(-2)	3.56(-2)	3.79(-2)	3.95(-2)
8	3	6.73(-2)	8.32(-2)	7.28(-2)	6.73(-2)	6.19(-2)
9	2	5.00(-2)	5.22(-2)	5.20(-2)	5.12(-2)	4.88(-2)
10	1.5	7.58(-2)	6.93(-2)	7.22(-2)	7.18(-2)	6.85(-2)
11	1	6.23(-2)	4.96(-2)	5.70(-2)	6.79(-2)	7.41(-2)
12	0.8	2.94(-2)	2.49(-2)	2.67(-2)	2.79(-2)	2.82(-2)
13	0.7	3.50(-2)	3.11(-2)	3.16(-2)	3.22(-2)	3.18(-2)
14	0.6	1.48(-1)	1.44(-1)	1.49(-1)	1.47(-1)	1.46(-1)
15	0.4	2.39(-1)	2.22(-1)	2.27(-1)	2.25(-1)	2.24(-1)
16	0.2	1.48(-1)	1.39(-1)	1.39(-1)	1.39(-1)	1.40(-1)
17	0.1	1.14(-2)	1.10(-2)	1.11(-2)	1.09(-2)	1.12(-2)
18	0.06	2.8(-4)	3.8(-4)	2.0(-4)	1.8(-4)	1.7(-4)
19	0.03	1.4(-5)	2.0(-5)	7.4(-6)	6.4(-6)	6.4(-6)
20	0.02	3.0(-6)	4.1(-6)	1.5(-6)	1.3(-6)	1.3(-6)
	0.01					
TOTALS		1.000	1.000	1.000	0.999	1.000

Table 14. Average Gamma-Ray Heating in Iron with Contributions from the Individual Components and Average Subcadmium Fluxes During the Two-Year Experiment

	SSC-1	SSC-2	0T	T/4	T/2	3T/4
Heating Rate	2.13(6)*	2.47(6)	6.47(5)	1.98(5)	5.07(4)	1.40(4)
% Prompt	14	14	7	7	6	5
% Fission-Product	9	9	4	4	3	2
% Non-Fission	77	77	89	89	91	93
Neutron Flux below 0.414 eV	2.64(12)†	3.06(12)	1.14(12)	9.25(10)	7.27(9)	2.29(9)
Heating Rate from Non-Fission / Neutron Flux below 0.414 eV	6.2(-7)	6.2(-7)	5.1(-7)	1.9(-6)	6.3(-6)	5.7(-6)

*Read 2.13 x 10^6 ergs/sec/gram, etc.
†Read 2.64 x 10^{12} neutrons/cm^2/sec, etc.

Table 15. Approximate Range of Group Axial Leakage Factors for the Gamma-Ray Components and Subcadmium Fluxes as Functions of Detector Location

	SSC	0T	T/4	T/2	3T/4
Prompt + Fission Product	0.76-0.81	0.70-0.80	0.71-0.75	0.71-0.74	0.71-0.76
Non-Fission	0.75-0.85	0.74-0.79	0.73-0.76	0.67-0.75	0.48-0.66
Neutron Flux below 0.414 eV	0.84	0.81	0.78	0.70	0.39

Finally, results of the photofission effects in the two-year irradiation experiment obtained with the photofission cross sections used by NBS (9) are presented in Table 16. Since the effective thresholds for photofission in both ^{238}U and ^{237}Np lie in the vicinity of 5.75 MeV, only the four gamma-ray groups IG=2-5 contribute to the effect. It can be concluded from Table 16 that photofission appears to be at most about a five percent effect, and that relative to neutron-induced fission the effect is at least three times more important in ^{238}U than in ^{237}Np.

Table 16. Estimated Photofission Reaction Rates in the Fission Foils and Comparison with Calculated Neutron-Induced Reaction Rates

	$^{238}U(\gamma,f)$	$^{238}U(n,f)^*$	$\frac{^{238}U(\gamma,f)}{^{238}U(n,f)}$	$^{237}Np(\gamma,f)$	$^{237}Np(n,f)^*$	$\frac{^{237}Np(\gamma,f)}{^{237}Np(n,f)}$
SSC-1	3.5(-14)†	1.86(-12)	1.9%	7.0(-14)	1.47(-11)	0.5%
SSC-2	4.0(-14)	2.16(-12)	1.9%	8.2(-14)	1.70(-11)	0.5%
0T	1.2(-14)	2.77(-13)	4.3%	2.5(-14)	1.98(-12)	1.3%
T/4	3.4(-15)	1.26(-13)	2.7%	6.9(-15)	1.18(-12)	0.6%
T/2	8.3(-16)	5.19(-14)	1.6%	1.7(-15)	6.38(-13)	0.3%

*Approximate values.
†Read 3.5×10^{-14} fissions/sec/nucleus, etc.

Conclusions

Although there are no measurements available with which to compare these calculations, it is felt that the gamma-ray fluxes presented in this report should be reasonably accurate (i.e., ~15%), and that the heating rates derived from thes fluxes should have comparable accuracy. The major contributor to the heating rate in the steel is the gamma rays born in the configuration as a result of non-fission reactions - presumably thermal-neutron captures in the steel but not necessarily at locations immediately next to the detector. Heating rates vary from about 0.23 watts/gram at the SSC to 0.0014 watts/gram at the 3T/4 location in the SPVC. Photofission effects in the fission foils are estimated to be about five percent or less for the ^{238}U foils and essentially negligible for the ^{237}Np foils.

REFERENCES

1. Maerker, R. E. and B. A. Worley, Activity and Fluence Calculations for the Startup and Two-Year Irradiation Experiments Performed at the Poolside Facility, NUREG/CR-3886, ORNL/TM-9265 (1984).

2. Simmons, G. L. and R. Roussin, SAILOR - A Coupled, Self-Shielded, 47 Neutron, 20 Gamma-Ray, P_3, Cross Section Library for Light Water Reactors, DLC-76, Radiation Shielding Information Center (1983).

3. Vondy, D. R., T. B. Fowler and G. W. Cunningham, III, The BOLD VENTURE Computation Program for Nuclear Reactor Core Analysis, ORNL-5711 (1981).

4. Rhoades, W. A. and R. L. Childs, An Updated Version of the DOT4 One- and Two-Dimensional Neutron/Photon Transport Code, ORNL-5851 (1982).

5. Roussin, R. W., BUGLE-80, A Coupled 47-Neutron, 20 Gamma-Ray, P_3, Cross Section Library for LWR Shielding Calculations, DLC-75, Radiation Shielding Information Center (1980).

6. Maienschein, F. C., "Prompt-Fission Gamma Rays," Engineering Compendium on Radiation Shielding, Vol. 1, Shielding Fundamentals and Methods, R. G. Jaeger, Editor-in-Chief, Springer-Verlag, New York, Inc. (1968).

7. Maienschein, F. C., "Fission-Product Gamma Rays," Ibid.

8. LaBauve, R. J. and D. C. George, PEFPYD - A Library of Aggregate Fission-Product Decay Data Derived from ENDF/B-IV, DLC-96, Radiation Shielding Information Center (1980).

9. Eisenhauer, C. M., private communication (1984).

NUREG/CR-4039
CRNL/TM-9440
Distribution Category R5

INTERNAL DISTRIBUTION

1-2. L. S. Abbott
3. C. A. Baldwin
4. D. G. Cacuci
5. P. W. Dickson, Jr. (Consultant)
6. D. M. Eissenberg
7. G. H. Golub (Consultant)
8. F. B. K. Kam
9-13. R. E. Maerker
14. F. C. Maienschein
15. A. P. Malinauskas
16. F. R. Mynatt
17. F. W. Stallmann
18. D. Steiner (Consultant)
19. C. R. Weisbin
20-24. B. A. Worley
25. A. Zucker
26. Central Research Library
27. ORNL Y-12 Technical Library-Document Reference Section
28. Laboratory Records
29. ORNL Patent Office
30. Laboratory Records - RC

EXTERNAL DISTRIBUTION

31. Office of Assistant Manager for Energy Research and Development, DOE-ORO, Oak Ridge, TN 37831.
32. C. Z. Serpan, Jr., Division of Engineering Technology, U.S. Office of NRC, MS-SS-1130, Washington, DC 20555.
33-34. Technical Information Center (TIC).
35-385. Given distribution as shown in NRC Category R5, Water Reactor Safety Research - Metallurgy and Materials (10 copies - NTIS).

NRC FORM 335 (11-81) U.S. NUCLEAR REGULATORY COMMISSION

BIBLIOGRAPHIC DATA SHEET

1. REPORT NUMBER (Assigned by DDC)
NUREG/CR-4039
ORNL/TM-9440

4. TITLE AND SUBTITLE (Add Volume No., if appropriate)
Gamma-Ray Characterization of the Two-Year Irradiation Experiment Performed at the Poolside Facility

2. (Leave blank)

3. RECIPIENT'S ACCESSION NO.

7. AUTHOR(S)
R. E. Maerker

5. DATE REPORT COMPLETED
MONTH: December YEAR: 1984

9. PERFORMING ORGANIZATION NAME AND MAILING ADDRESS (Include Zip Code)
Engineering Physics and Mathematics Division
Oak Ridge National Laboratory
P.O. Box X
Oak Ridge, TN 37831

DATE REPORT ISSUED
MONTH: January YEAR: 1985

6. (Leave blank)

8. (Leave blank)

12. SPONSORING ORGANIZATION NAME AND MAILING ADDRESS (Include Zip Code)
U.S. Nuclear Regulatory Commission
Washington, D.C. 20555

10. PROJECT/TASK/WORK UNIT NO.

11. FIN NO.
B0415

13. TYPE OF REPORT
TOPICAL

PERIOD COVERED (Inclusive dates)
July - September 1984

15. SUPPLEMENTARY NOTES

14. (Leave blank)

16. ABSTRACT (200 words or less)

Average gamma-ray group fluence rates are calculated for each of the three exposures in the two-year metallurgical blind test experiment at the ORR-Poolside Facility in Oak Ridge, thus completing the characterization of the radiation field for this experiment, which is intended to serve as an international metallurgical benchmark. Heating rates in the steel derived from these calculations varied from about 0.23 watts/gram in the simulated surveillance capsule to 1.4 milliwatts/gram at the three-quarters depth location in the simulated pressure vessel capsule, with secondaries arising from non-fission reactions in the core and ex-core steel contributing between seventy-seven and ninety-three percent of the total. Contributions from photofission to fission foil activities are estimated to be less than five percent of those previously calculated arising from neutron-induced fission.

17. KEY WORDS AND DOCUMENT ANALYSIS

17a. DESCRIPTORS

17b. IDENTIFIERS/OPEN-ENDED TERMS

18. AVAILABILITY STATEMENT
Unlimited

19. SECURITY CLASS (This report)
Unclassified

21. NO. OF PAGES
34

20. SECURITY CLASS (This page)
Unclassified

22. PRICE
$